Progress In Electromagnetics Research M, Vol. 33, 69–82, 2013

EXPERIMENTAL RESULTS FOR MICROWAVE TOMOGRAPHY IMAGING BASED ON FDTD AND GA

Abas Sabouni[1, *] and Sima Noghanian[2]

[1]Department of Electrical Engineering and Physics, Wilkes University, Wilkes-Barre, PA 18766, USA

[2]Department of Electrical Engineering, University of North Dakota, Grand Forks, USA

Abstract—The authors recently presented a novel microwave tomography method for creating quantitative images of the electromagnetic properties of the interior of unknown objects [1]. This method is based on a time-domain inverse solver which uses the multi-illumination technique and includes the dispersive and heterogeneous characteristic of the object. The Frequency Dependent Finite Difference Time Domain ($(FD)^2TD$) and Genetic Algorithm (GA) technique were utilized for determining unknown characteristics of the object. In the present paper, the calibration of measured data are described and image reconstruction results for preliminary experiments performed at the University of Manitoba's Microwave Tomography Laboratory and at the Institut Frsenel are presented.

1. INTRODUCTION

MicroWave Tomography (MWT) has received intense attention as an imaging modality. Therefore, extensive research has been conducted in this field during the last 40 years. This is due to the versatility and suitability of this imaging technique for a wide range of applications such as industrial non-destructive testing [2], medical imaging [3], and through-wall imaging [4]. The use of electromagnetic fields for the purpose of quantitatively determining the inner structure of objects leads to inverse mathematical problems.

The challenge of inverse problems, however, is that it involves the solution of an ill-conditioned non-linear problem which is often

Received 6 August 2013, Accepted 26 September 2013, Scheduled 27 September 2013

* Corresponding author: Abas Sabouni (abas.sabouni@wilkes.edu).

computationally intensive and might not have a unique solution [5]. The non-linearity is due to the fact that at the frequencies of the microwave radiation, the electromagnetic waves scatter multiple times, refract through and diffract around the Object of Interest (OI), and generally do not follow straight paths within the imaging region. Iterative techniques are among the best options for solving the non-linear inverse scattering problems and for producing quantitative images using permittivity and conductivity. In iterative techniques, the solution is found by minimizing the norm of the error with respect to the scattered field's value (cost-function). There are two different categories of iterative approaches that have been successfully used to solve the inverse scattering problem. These two approaches are also distinguished by the absence of, or the use of, a forward solver. In the first approach the cost-function is defined based on both scattered fields outside of the object and total fields inside the object [6–8]. However, the number of unknowns in this approach is greater than that in second approach, and therefore, it requires much more iterations to converge [6]. The second approach for solving the inverse scattering problem measures the scattered field outside the object and tries to minimize the error calculated for a possible solution using a forward solver [9, 10]. This approach is computationally intensive because the system of equations that is used to calculate the scattered fields (whether using Integral Equations (IE) or Partial Differential Equations (PDE)), has to be built at each iteration. Furthermore, in order to minimize the cost-function and retrieve the unknown objects from the measurements, different deterministic (local optimization) [11–15] and stochastic (global optimization) [16–19] approaches have been proposed. The local-based optimization imaging techniques produce accurate and reliable results only if the starting trial solution is not far from the real solution. In many practical cases, it is not possible to guess the proper initial point, and therefore, the optimization may return a non-true solution that locally minimizes the cost function. The stochastic approaches are potentially able to obtain the global minimum which most probably corresponds to the true solution. In addition, they are able to reach the global minimum of the cost-function regardless of the starting point. Recently, the authors developed the numerical simulation method based on Frequency Dependent Finite Difference Time Domain ($(FD)^2TD$) and Genetic Algorithm (GA) for creating a map of dielectric properties of an object of interest [1]. The contribution of this paper is to demonstrate the ability of proposed technique by utilizing it to reconstruct images using measured noisy data.

The paper is organized as follows. In next section, we explain

the hardware setup required to collect the necessary field for MWT imaging and also different calibrations needed to be performed before inverting the scattered field data. Then we present the image results from experimental data followed by conclusion in Section 3.

2. EXPERIMENTAL INVERSION RESULTS

2.1. Experimental Data from University of Manitoba Microwave Tomography System

The University of Manitoba (UM) imaging group recently developed and constructed an MWT prototype. This system includes a plexiglass cylindrical shell with 44 cm diameter and 50.8 cm height. A circular array of 24 antennas is mounted inside the plexiglass cylinder. A two-port Agilent 8363B PNA-Series Vector Network Analyzer (VNA) is used to measure the S-parameters between each antenna pairs, and a 2×24 mechanical switch is used for connecting two ports of network analyzer into 24 antennas. The data acquisition is automated, and for each frequency the measurement takes about one minute. For more details about this system see [20]. Fig. 1 shows the UM MWT setup with 24 Vivaldi antennas. As an initial phantom experiment, we utilized a wooden block with square cross-section and $87 \times 87 \times 300\,\text{mm}^3$ dimensions. The relative permittivity of the wood is around 1.8 at 3 GHz, and the conductivity is very low. We considered the wooden block as a loss-less material in simulation. The wood was placed at the center of the UM MWT chamber within air, as shown in Fig. 1. The measurement was taken at the frequencies between 3–6 GHz, with step of 0.5 GHz.

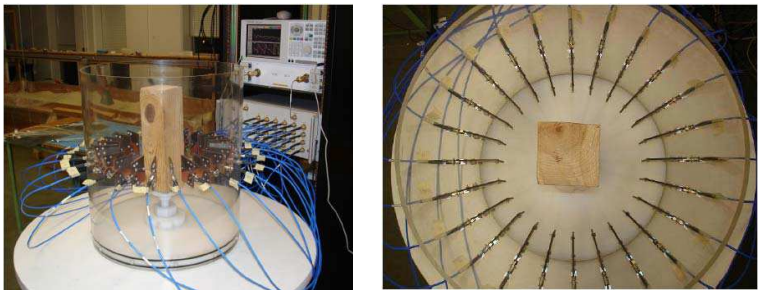

(a) (b)

Figure 1. UM MWT system using 24 Vivaldi antennas, (a) side view, (b) top view [20].

2.1.1. Calibration

It is well-known that in MWT the measured data must be calibrated. This is due to the elimination of antennas in the inversion algorithm. Calibration can be divided into "hardware calibration", "field calibration", and "model calibration". Hardware calibration is the process to compensate the systematic errors in the network analyzer, adapters, and cables during measurements [21, 22]. Hardware calibration has a significant role in the reliability and repeatability of the measure data sets and is an important prerequisite of field calibration. Field calibration is used to determine the electric field intensity values from measurements of S-parameters by the VNA. VNA has a unity output voltage and the field component of interest can be assumed to be proportional to the induced voltage at the port of the antenna. Therefore:

$$\left(E_{nm}^{\text{measured}}\right)_{\text{OI}} = \text{AF} \cdot \left(S_{nm}^{\text{measured}}\right)_{\text{OI}} \tag{1}$$

where $(E_{nm}^{\text{measured}})_{\text{OI}}$ is the measured electric field for the OI object when the antenna number m is transmitting and antenna number n is receiving the signal. $(S_{nm}^{\text{measured}})_{\text{OI}}$ is the transmission coefficient from S parameters for the OI object, collected by VNA when the transmitting antenna is connected to port m and receiving antenna is connected to port n. The factor AF refers to the factor that would convert the S_{nm} measurement from incident field or scattered field of a reference object to its associated electric field values:

$$\text{AF} = \frac{(E_{nm}^{\text{simulated}})_{ref}}{(S_{nm}^{\text{measured}})_{ref}} \tag{2}$$

where $(E_{nm}^{\text{simulated}})_{ref}$ is the simulated electric field for the reference (known) object when the antenna number m is transmitting and antenna number n is receiving the signal. $(S_{nm}^{\text{measured}})_{ref}$ is the transmission coefficients from S parameters for the reference object. The error in the approximation in (1) becomes zero only if $(S_{nm}^{\text{measured}})_{\text{OI}} = (S_{nm}^{\text{measured}})_{ref}$. To perform the field calibration, we first calibrated the MWT system using the AF correction coefficient (2). For this purpose, we simulated the entire MWT system using the 3D WIPL-D solver (Fig. 2) [23]. Fig. 3 compares the transmission coefficient values for the 3D simulation data and the raw measured data at 3 and 6 GHz for the 87 mm square wooden block when antenna number 1 is transmitting. From the Fig. 3, it is observed that the simulation and measurement results do match at a 3 GHz, but not at 6 GHz. This means that the calibration factor is a function of frequency, as expected. Table 1 shows the average error between the

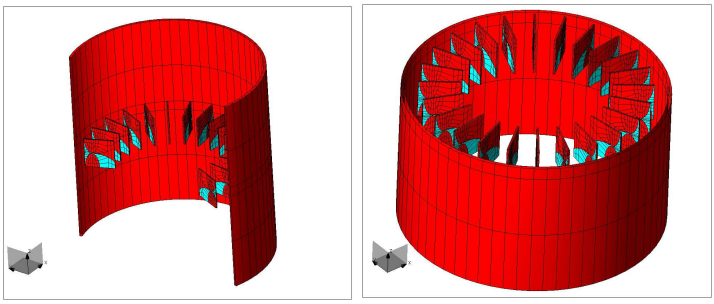

(a) (b)

Figure 2. Simulation geometry of the MWT chamber with 24 Vivaldi antennas.

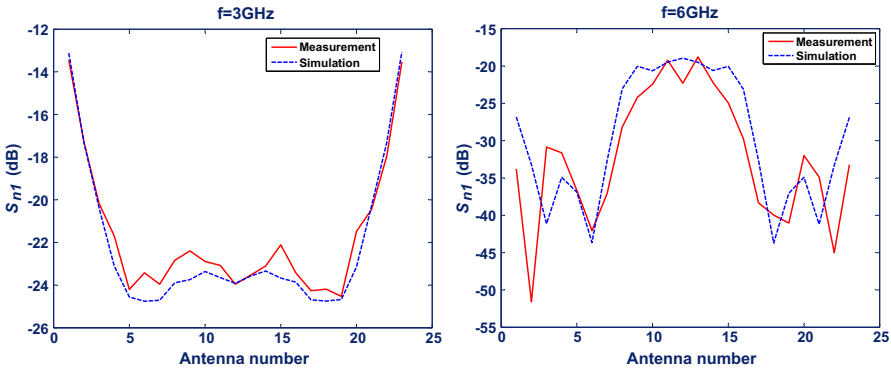

(a) (b)

Figure 3. Amplitude of S_{n1} vs. antenna number at (a) 3 GHz, and (b) 6 GHz.

Table 1. Total error in S_{n1} for UMMWT chamber.

Frequency (GHz)	3	3.5	4.5	5	6
Amplitude (dB)	0.47	2.25	1.54	0.54	2.42
Phase (°)	0.80	1.65	1.12	1.74	1.36

transmission coefficient values from simulation and measured data at different frequencies. Therefore, the model calibration is necessary to compensate for the discrepancy between the measured and simulated field values.

Model calibration is the process of applying a correction coefficient

to the measured data to correct the assumption in modeling and inversion algorithm. This correction coefficient can be obtained by comparing the simulated field values at the observation points for an assumed model with the measured field value from the same model at those receiver points. This correction factor is then applied to the measured scattered field data to compensate for the discrepancy between the measured and simulated field values. In order to calculate this factor, either the incident field or the scattered field of a known reference object has been suggested and used by researchers. Different reference objects such as an empty chamber (incident field) [24], a metallic cylinder [20, 25], nylon, or polyvinyl chloride [26], have been successfully used for different imaging algorithms.

Here, as an example, we have utilized two Perfect Electric Conductor (PEC) cylinders with diameters of 38.4 mm and 50.9 mm, as well as incident field as a reference object. We used these reference objects due to the ease of characterization. Fig. 4 compares the simulated and calibrated data for different reference objects at 3 GHz and 3.5 GHz. It should be noted that at 3 GHz, where the coupling between antennas is low [20], the calibrated data is well matched with the simulation, compared to the results obtained at 3.5 GHz. However, even at 3 GHz, where the coupling seems to be minimal, there is still some discrepancies between simulated and measured fields, which might be due to the assumption of a plane-wave incident field (in inverse simulation) as a source instead of real antennas' fields. Besides, at other frequencies where the antenna-coupling was high the results

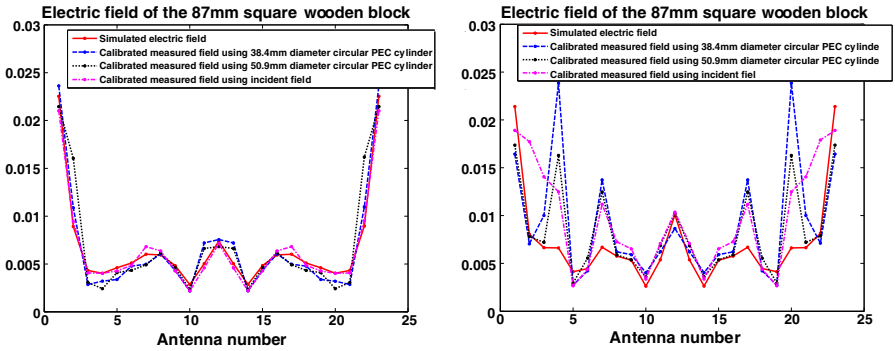

Figure 4. Magnitude comparison of simulated and calibrated electrical field for different reference objects at (a) 3 GHz, and (b) 3.5 GHz.

were much worse. This means that the antenna coupling effects are not entirely removable by the calibration procedure, and they are major sources of error. Note that the 3D WIPL-D software is employed to calculate the calibration factor only, and for the inversion algorithm a 2D ((FD)^{2}TD) code is used as a forward solver.

2.1.2. Inversion Results

The single-frequency 3 GHz reconstructed image of the wooden block object is shown in Fig. 5. For image reconstruction, we considered four different transmission angles (0°, 90°, 180°, and 270°) and 23 receiving angles within $15° \leq \Phi \leq 345°$ with respect to the transmitter (Φ is the angle of the observation point from the axis of the incident wave). The reconstructed map of permittivity is generally correct; however, in some parts the exact values are not obtained, but the results are close to real values. To obtain usable frequencies for our inverse scattering experiment, we selected those frequencies where the coupling was minimum [20]. We expect that when the MWT system is filled with a matching material, the antenna coupling will become significantly less noticeable due to losses. In this example as *a-priori* information, we considered the reconstructed relative complex permittivity to be within physical ranges $\epsilon_r \geq 1.0$ and $\sigma = 0.0\,\mathrm{S/m}$, with 1 decimal point accuracy. As an image quality indicator, we define the mean-squared

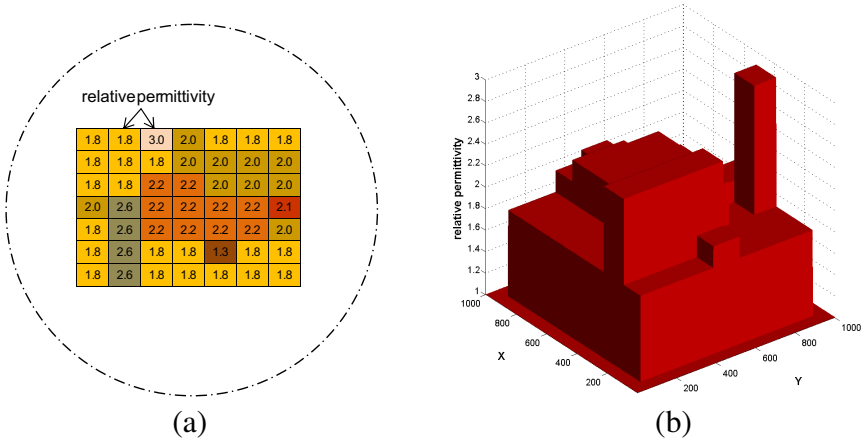

Figure 5. Reconstructed image of wooden block (map of permittivity), (a) 2D view, and (b) 3D view.

error between the true image and the reconstructed image as follows:

$$\text{Error} = \frac{\sum_i \sum_j \frac{|\epsilon_{r(\text{reconstructed image})} - \epsilon_{r(\text{true image})}|^2}{|\epsilon_{r(\text{true image})}|^2}}{\text{number of cells}} \tag{3}$$

where i and j are the cell numbers in the x and y directions, respectively, and ϵ_r is the relative permittivity. In this example the Error at 3 GHz is $\approx 4\%$ assuming a constant permittivity inside the wooden block. However, we speculate that the wooden block is a heterogeneous object and the permittivity varies within the block. Therefore, the reconstructed permittivity map is probably closer to the real values.

2.2. Experimental Data from Institut Frsenel's MWT System

In order to test the *blind* inversion capabilities of the proposed algorithm for solving the inverse scattering problem, we present inversion results from 2D experimental scattering data collected by the Institut Frsenel. In 2005, the Centre Commun de Ressources Micro-Ondes (CCRM) at the Institute Fresnel in Marseilles, France provided an invaluable public database of experimental multi-frequency electromagnetic field data from multiple scatterers. This database has been used by many researchers around the world for evaluating their MWT algorithms. For more details about the measurement data including system dimensions, transmitting and receiving antennas, frequencies, polarizations, and targets, see reference [27]. This data set was collected for Transverse Electric (TE) and Transverse Magnetic (TM) polarizations in free-space. For this measurement, a double ridged horn antenna was used in an anechoic chamber setup with a frequency of 1–18 GHz. Antenna was 1.67 meters away from the center of the imaging region. The two antennas mechanically rotated around the OI and collected the data at 241 positions per transmitter. The measured data was then calibrated such that the transmitted field by antennas can be approximated by a plane-wave and the effects of the antenna's radiation patterns are removed. To calibrate this data, the offset calibration method was used [28]. In this type of calibration, a single correction factor is used for all transmitter/receiver pairs. Such a calibration has provided good results in far-field measurement systems [29].

Figure 6(a) shows the cross-section of a foam cylinder (SAITEC SBF 300) with 80 mm diameter and relative permittivity of 1.45 ± 0.15. A plastic cylinder (berylon) with diameter of 31 mm and relative

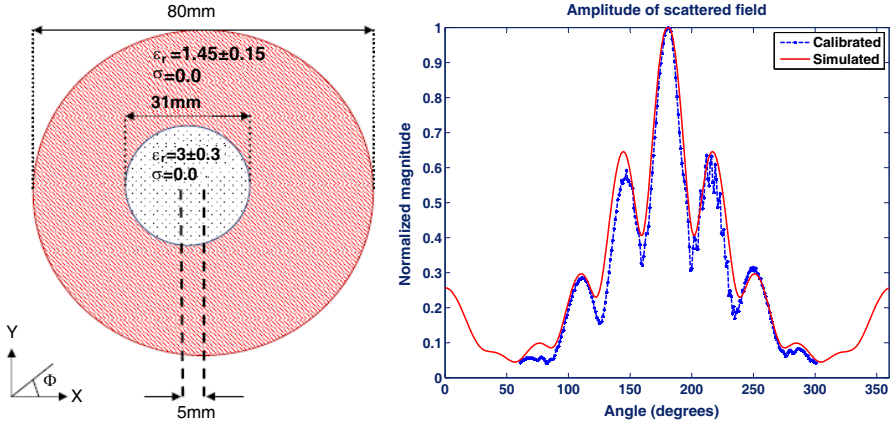

Figure 6. Geometry for Fresnel data set FoamDielint, (a) schematic of the scattering cylinders, (b) comparing the calibrated and simulated scattered field at 8 GHz where the transmitter antenna is positioned at 180°.

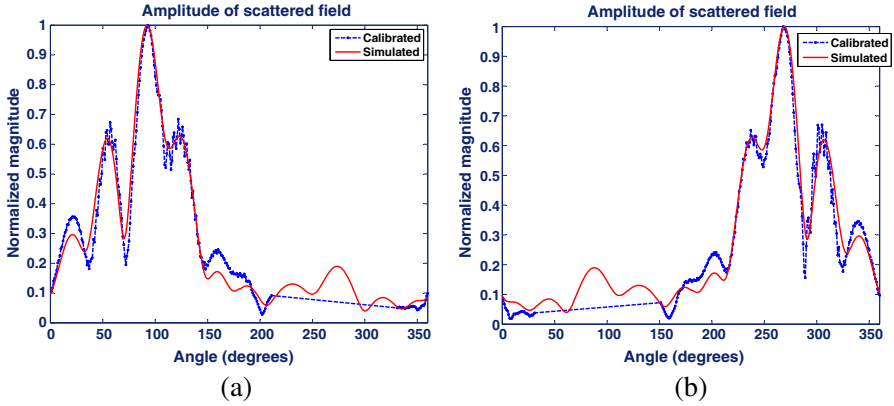

Figure 7. Comparing the calibrated and simulated data at 8 GHz where the transmitter antenna is positioned at (a) 90°, and (b) 270°.

permittivity of 3 ± 0.3 is placed inside the foam cylinder, 5 mm away from the center. The data for this setup was collected for 8 transmitters and 241 receivers per transmitter at 9 frequencies, in the bandwidth of 2–10 GHz, with 1 GHz steps. Figs. 6(b) and 7(a), (b) compare the calibrated scattered fields given by simulation and measurement, at 8 GHz, when the transmitter antennas are positioned at $\Phi = 90°$, 180°,

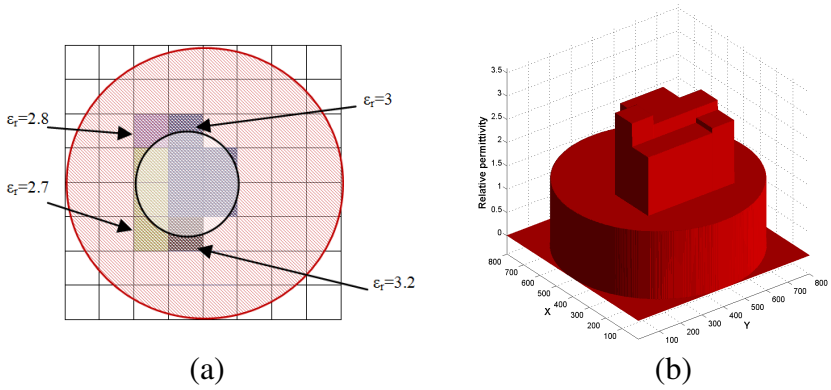

Figure 8. Reconstruction of Fresnel data set FoamDielint (map of permittivity), (a) 2D view, and (b) 3D view.

and 270°. The inversion of this dataset using the $(FD)^2TD/GA$ method is shown on the grid of 8×8 in Fig. 8. We considered that the location, size, and material of the foam cylinder is known. Therefore, the material for those cells outside of the foam cylinder and circular shape of the boundary are known. We also constrained the inversion process for loss-less material and the relative permittivity of the scatterers to be in the range of 1–10 ($1 < \epsilon_r \leq 10$). We utilized multiple frequencies in our techniques for the frequency band between 2–8 GHz in 2 GHz steps. While the $(FD)^2TD$ method has been used in the forward solver, the data for all frequencies are used simultaneously. As a proof of concept, we considered only one transmitter at $\Phi = 0°$ and 241 receiver antennas within $60° \leq \Phi \leq 300°$. However, it is expected that using multi-view techniques will provide significantly better results. The search space area was divided into 64 square cells, with 1 cm side. As it can be seen in Fig. 8, the algorithm accurately reconstructs the location of the target. In terms of dielectric properties of the object, the reconstructed image is close enough to the actual one, but there are still differences in some parts of the image. In this example the Error at 2 GHz is $\approx 7.6\%$. For this shape of the scatterer, there is a discrepancy between the actual image and the reconstructed image. This inaccuracy in the result of shape and dielectric properties can be decreased if the cell size is decreased at the price of increasing the runtime.

According to the results obtained with the Institut Frsenel's MWT system, a target of 1 cm was imaged, which corresponds to a resolution of $\lambda/9$ at 2 GHz. This high resolution is achieved through the use of

far-field data as well as the use of a nonlinear inversion algorithm that accounts for multiple scattering. In previous example, we were able to detect a target of 1.24 cm which corresponds to a resolution of $\lambda/6$ at 3 GHz using near-field data. In fact, as it has been suggested in [30, 31] that the true resolution limit for MWT is governed by the achievable signal-to-noise ratio of the measurements and not the wavelength. It is important to note that the noise is not simply receiver thermal noise and that the "modeling errors" are much more important sources of noise. Therefore, while the resolution limit for MWT technology is not currently known, perhaps improving the data acquisition techniques, measurement calibration methods, and imaging algorithms would allow for significant improvement in the resolution of MWT.

3. CONCLUSION

We have introduced a novel method based on stochastic approaches without any simplification in the non-linear wave equation, in order to circumvent the inverse problem. The proposed technique deals with an object that has a complex distribution of dielectric properties and provides an image of permittivity and conductivity, as well as a quantitatively reconstructed frequency-dependent profile of these properties. This method is based on the time domain iterative approach to solve an inverse scattering problem that is efficient and accurate for dispersive and heterogeneous media. The proposed technique is capable of using multi-frequency and multi-illumination techniques for the reconstruction of the dielectric properties profile to improve image quality. We presented preliminary image reconstruction results for experiments performed by the University of Manitoba's and the Institut Frsenel's MWT systems.

Although further analysis should be performed for a complete assessment of the methodology, the obtained results indicate the potential of MWT as an effective imaging technique deserving further investigations.

ACKNOWLEDGMENT

The authors would like to acknowledge the financial support of Wilkes University, Natural Sciences and Engineering Research Council of Canada, CancerCare Manitoba, and University of North Dakota.The authors would like to thank Dr. M. Ostadrahimi for collecting the measurement data. Also constructive discussions with Dr. S. Pistorius, Dr. L. Shafai, and Dr. P. Thulasiraman are greatly appreciated.

REFERENCES

1. Sabouni, A., S. Noghanian, and S. Pistorius, "A global optimization technique for microwave imaging of the inhomogeneous and dispersive breast," *Canadian Journal of Electrical and Computer Engineering*, Vol. 35, No. 1, 15–24, 2010.
2. Pastorino, M., S. Caorsi, and A. Massa, "A global optimization technique for microwave nondestructive evaluation," *IEEE Transactions on Instrumentation and Measurement*, Vol. 51, No. 4, 666–673, 2002.
3. Meaney, P. M., M. W. Fanning, T. Raynolds, C. J. Fox, Q. Fang, C. A. Kogel, S. P. Poplack, and K. D. Paulsen, "Initial clinical experience with microwave breast imaging in women with normal mammography," *Academic Radiology*, Vol. 14, No. 2, 207–218, 2007.
4. Song, L. P., C. Yu, and Q. H. Liu, "Through-wall imaging (TWI) by radar: 2-D tomographic results and analyses," *IEEE Transactions on Geoscience and Remote Sensing*, Vol. 43, No. 12, 2793–2798, 2005.
5. Hansen, P. C., *Rank-deficient and Discrete Ill-posed Problems: Numerical Aspects of Linear Inversion*, SIAM, Philadelphia, PA, 1998.
6. Barkeshli, S. and R. G. Lautzenheiser, "An iterative method for inverse scattering problems based on an exact gradient search," *Radio Science*, Vol. 29, 1119–1130, 1994.
7. Kleinman, R. E. and P. M. van den Berg, "A modified gradient method for two-dimensional problems in tomography," *Journal of Computational and Applied Mathematics*, Vol. 42, No. 1, 17–35, 1992.
8. Van den Berg, P. M. and R. E. Kleinman, "A contrast source inversion method," *Inverse Problems*, Vol. 13, No. 6, 1607–1620, 1997.
9. Chew, W. and Y. Wang, "Reconstruction of two-dimensional permittivity distribution using the distorted born iterative method," *IEEE Transactions on Medical Imaging*, Vol. 9, No. 2, 218–225, 1990.
10. Caorsi, S., M. Donelli, and A. Massa, "Detection, location, and imaging of multiple scatterers by means of the iterative multiscaling method," *IEEE Transactions on Microwave Theory and Techniques*, Vol. 52, No. 4, 1217–1228, 2004.
11. Habashy, T. M. and A. Abubakar, "A general framework for constraint minimization for the inversion of electromagnetic

measurements," *Progress In Electromagnetics Research*, Vol. 46, 265–312, 2004.

12. Bozza, G., C. Estatico, M. Pastorino, and A. Randazzo, "An inexact newton method for microwave reconstruction of strong scatterers," *IEEE Antennas and Wireless Propagation Letters*, Vol. 5, No. 1, 61–64, 2006.
13. Franchois, A. and A. G. Tijhuis, "A quasi-Newton reconstruction algorithm for a complex microwave imaging scanner environment," *Radio Science*, Vol. 38, No. 2, 1–13, 2003.
14. Joachimowicz, N., J. Mallorqui, J. C. Bolomey, and A. Broquets, "Convergence and stability assessment of Newton-Kantorovich reconstruction algorithms for microwave tomography," *IEEE Transactions on Medical Imaging*, Vol. 17, No. 4, 562–570, 1998.
15. Franchois, A. and C. Pichot, "Microwave imaging-complex permittivity reconstruction with a Levenberg-Marquardt method," *IEEE Transactions on Antennas and Propagation*, Vol. 45, No. 2, 203–215, 1997.
16. Pastorino, M., "Stochastic optimization methods applied to microwave imaging: A review," *IEEE Transactions on Antennas and Propagation*, Vol. 55, No. 3, 538–548, 2007.
17. Caorsi, S., A. Massa, M. Pastorino, and M. Donelli, "Improved microwave imaging procedure for nondestructive evaluations of two-dimensional structures," *IEEE Transactions on Antennas and Propagation*, Vol. 52, No. 6, 1386–1397, 2004.
18. Donelli, M. and A. Massa, "Computational approach based on a particle swarm optimizer for microwave imaging of two-dimensional dielectric scatterers," *IEEE Transactions on Microwave Theory and Techniques*, Vol. 53, No. 5, 1761–1776, 2005.
19. Donelli, M., G. Franceschini, A. Martini, and A. Massa, "An integrated multiscaling strategy based on a particle swarm algorithm for inverse scattering problems," *IEEE Transactions on Geoscience and Remote Sensing*, Vol. 44, No. 2, 298–312, 2006.
20. Gilmore, C., P. Mojabi, A. Zakaria, M. Ostadrahimi, C. Kaye, S. Noghanian, L. Shafai, S. Pistorius, and J. LoVetri, "A wideband microwave tomography system with a novel frequency selection procedure," *IEEE Transactions on Biomedical Engineering*, Vol. 57, No. 4, 894–904, 2010.
21. Meaney, P., K. Paulsen, A. Hartov, and R. Crane, "An active microwave imaging system for reconstruction of 2-D electrical property distributions," *IEEE Transactions on Biomedical Engineering*, Vol. 42, No. 10, 1017–1026, 1995.

22. Eyraud, C., J. M. Geffrin, A. Litman, P. Sabouroux, and H. Giovannini, "Drift correction for scattering measurements," *Applied Physics Letters*, Vol. 89, 2441041–2441043, 2006.
23. Kolundzija, B., J. Ognjanovic, M. Tasic, D. Olcan, M. Paramentic, D. Sumic, M. Kostic, and M. Paviovic, "WIPL-D pro V7.1: 3D electromagnetic solver," *Tech. Rep.*, WIPL-D Ltd, Europe, 2009.
24. Meaney, P., M. Fanning, D. Li, S. Poplack, and K. Paulsen, "A clinical prototype for active microwave imaging of the breast," *IEEE Transactions on Microwave Theory and Techniques*, Vol. 48, No. 11, 1841–1853, 2000.
25. Geffrin, J. and A. Joisel, "Comparison of measured and simulated incident and scattered fields in a 434 MHz scanner," *Proceedings of the 22th URSI General Assembly*, 2002.
26. Gunnarsson, T., "Quantitative microwave breast phantom imaging using 2.45 GHz system," *International Union of Radio Science General Assembly*, 2008.
27. Geffrin, J. M., P. Sabouroux, and C. Eyraud, "Free space experimental scattering database continuation: Experimental set-up and measurement precision," *Inverse Problems*, Vol. 21, S117–S130, 2005.
28. Franchois, A., A. Joisel, C. Pichot, and J. C. Bolomey, "Quantitative microwave imaging with a 2.45 GHz planar microwave camera," *IEEE Transactions on Medical Imaging*, Vol. 17, No. 4, 550–561, 1998.
29. Belkebir, K. and M. Saillard, "Special section on testing inversion algorithms against experimental data," *Inverse Problems*, Vol. 17, 1565–1571, 2001.
30. Meaney, P., K. Paulsen, A. Hartov, and R. Crane, "Microwave imaging for tissue assessment: Initial evaluation in multitarget tissue-equivalent phantoms," *IEEE Transactions on Biomedical Engineering*, Vol. 43, 878–890, 1996.
31. Semenov, S., R. Svenson, A. Bulyshev, A. Souvorov, A. Nazarov, Y. Sizov, V. Posukh, A. Pavlovsky, P. Repin, and G. Tatsis, "Spatial resolution of microwave tomography for detection of myocardial ischemia and infarction-experimental study on two-dimensional models," *IEEE Transactions on Microwave Theory and Techniques*, Vol. 48, No. 4, 538–544, 2000.